Energy 198 (2020) 117294

Contents lists available at ScienceDirect

Energy

journal homepage: www.elsevier.com/locate/energy

Effect of conjugate heat exchange of flame holder on laminar premixed flame stabilization in a meso-scale diverging combustor

Jianlong Wan , Haibo Zhao *

State Key Laboratory of Coal Combustion, School of Energy and Power Engineering, Huazhong University of Science and Technology, Wuhan, 430074, China

ARTICLE INFO

Article history:
Received 18 July 2019
Received in revised form
21 February 2020
Accepted 29 February 2020
Available online 4 March 2020

Keywords:
Flame holder
Diverging combustor
Heat exchange
Flame stability
Pulsating flame

ABSTRACT

The present work investigates the effect of heat exchange of flame holder on the premixed flame stabilization in a diverging channel through numerical simulation. When the heat exchange of flame holder exists, the flame can remain stable and presents a "V" shape. A majority of the heat flux that enters the flame holder is used to preheat the incoming fresh mixture, which can induce and enhance the initiation of reactions. Moreover, three different zones are found and defined, including the free reaction zone, the quenching zone, and the enhanced reaction zone. However, when the heat exchange of flame holder is absent, the flame pulsates up and down instead of remaining stable, and shows a cone "Λ" shape. Subsequently, the pulsating mechanisms of flame are quantitatively analyzed in terms of local flow velocity, the angle between flow direction and flame front, and the stretch rate. The pulsation is a dynamic process where the flame speed self-adjusts to match the normal component of flow velocity. In summary, the present study indicates that the heat exchange of flame holder can significantly suppress the flame instability and improve the flame anchoring performance.

1. Introduction

In the micro- and meso-scale combustors, the flame is easy to lose stability owing to the short residence time of fuel mixture and the large surface-area-to-volume ratio [1]. Many unstable flame propagation modes were observed. For example, Maruta et al. [2] experimentally observed the flame with repetitive extinction and ignition (FREI) in a narrow tube with a temperature gradient, which was further reproduced by Alipoor and Mazaheri [3] via numerical simulation. Xu and Ju [4] experimentally observed the X-shape spinning flame in a meso-scale diverging tubular combustor, which was also recently observed by Wan et al. [5]. Deshpande and Kumar [6] found the spinning flame with high frequency at a suitable flow rate and an equivalence ratio in a meso-scale tube combustor with three steps. Akram and Kumar [7] experimentally observed the negatively stretched and positively stretched flame behaviors in a meso-scale diverging combustor. These unstable flames impede the extensive application of combustors with diverging structure. (see Table 1).

Various special structures were adopted to improve the flame stability. For instance, Kuo and Ronney [8] used the "Swiss-roll" configuration to extend the flammability limits in small combustors via excellently preheating the fresh fuel mixture. Federici and Vlachos [9] pointed out that the heat recirculation effect can obviously expand the blow-off limit in a small combustor with single-pass heat recirculation. Veeraragavan [10] found that the "hot pockets" in the solid wall with orthotropic thermal conductivity can improve the flame stability in a plate combustor. The inert porous media can also significantly expand the operating ranges of inlet velocity and equivalence ratio in the micro- and meso-scale burners [11–15]. Moreover, the flow recirculation generated behind the bluff body or in the cavity also has great anchoring effects on the flame [16–19]. Yang et al. [17] found that the hydrogen/air premixed flame can keep stable within a wide operating range in a micro combustor with one backward facing step. Wan et al. [19,20] developed different combustors with bluff-body or cavity, and both experimental and numerical results indicated that the blow-off limits are indeed enlarged and the flames are well anchored. Furthermore, the enhanced flame-wall coupling effect can also improve the flame stability. Baigmohammadi et al. [21] pointed out that the wire insertion can significantly improve the flame stabilization via enhancing the flame-wall coupling effect in a micro combustor with the backward facing step. Yang et al. [22] found that the block insertion can improve the flame stability and

* Corresponding author. State Key Laboratory of Coal Combustion, Huazhong University of Science and Technology, 1037 Luoyu Road, Wuhan, 430074, China.
E-mail address: hzhao@mail.hust.edu.cn (H. Zhao).

https://doi.org/10.1016/j.energy.2020.117294
0360-5442/

Table 1
Boundary condition of CFD simulations.

Inner surfaces	Chemically inert and no-slip
Heat fluxes	Fourier's law
Solid material	Quartz glass (2.0 W m^{-2} K^{-1}) [4]
Combustor inlet	Uniform concentration and velocity
Combustor exit	Neumann boundary
Heat loss rate	$q = h_s(T_{W,o} - T_\infty) + \varepsilon_s\sigma_s(T_{W,o}^4 - T_\infty^4)$
$T_{w,o}$	Temperature of outer wall surface
T_∞	Ambient temperature (300 K)
h_s	Natural convection coefficient (5.0 W m^{-2} K^{-1}) [28]
ε_s	Surface emissivity (0.92) [29]
σ_s	Stephan-Boltzmann constant (5.67×10^{-8} W m^{-2} K^{-4})

increase the average temperature of the combustor outer wall.

The above flame-anchoring methods were mostly applied to combustors with constant channel width. However, many practical combustors have variable chamber width [4], and the relevant studies on improving the flame stability in the variable channel width were rare in literatures. Recently, we developed a diverging tube combustor with a cylindrical flame holder. On the technical aspect, it can be used as a heat source for the thermophotovoltaic system. On the theoretical aspect, the developed diverging combustor (without external heating) can act as a model for further study of the flame-wall coupling effect on the flame dynamics, which can also be easily reproduced by numerical simulation. Our experimental results presented that the cylindrical flame holder can remarkably improve the flame stabilization (the spinning flame did not occur) and make the flame keep symmetrical in a wide operating range [5]. The flame-anchoring mechanisms in this combustor were further revealed in terms of conjugate heat exchange and preferential transport effect via simulation [23]. These works indicated that heat exchange between the flame and the holder can significantly expand the operating range of stable flame and influence the flame-anchoring performance. However, the underlying mechanisms of the suppressive effect of flame holder on the unstable flame in the diverging channel have not been revealed. The present work quantitatively compared the flame propagation characteristics in the diverging tube combustor with/without the heat exchange effect of flame holder. Interestingly, the flame pulsates up and down in the case without the heat exchange of flame holder, and the pulsating mechanisms are systematically discussed. This work can provide theoretical basis for further suppressing the unstable flame and improving the flame stabilization via enhancing the flame-wall coupling effect, which is the main objective of the present study.

2. Numerical methods

2.1. Geometric model of the combustor

Fig. 1 shows geometrical structure the of the meso-scale diverging combustor with a cylindrical flame holder, which was fabricated by the transparent quartz glass [5]. The combustor with an axial symmetry structure is vertically installed. The diameter of the cylindrical flame holder is 2.0 mm. The thickness (δ) of the combustor wall is 1.0 mm, and the gap distance at the combustor inlet is 1.0 mm. The total height of the combustor is 150.0 mm.

2.2. Mathematical model

In this study, the flow velocity at the inlet of the combustor is 3 m/s (the corresponding Reynolds number (*Re*) of the cold fuel mixture is 120). Moreover, experimental results showed that the flame remains laminar in the present combustor [5,23]. Therefore, the laminar flow and unsteady-state models are adopted in the current computation. The governing equations are displayed as follows:

Continuity equation
$$\frac{\partial \rho}{\partial t} + \frac{\partial}{\partial x}(\rho u) + \frac{\partial}{\partial y}(\rho v) = 0 \tag{1}$$

Momentum equations:
$$\frac{\partial(\rho u)}{\partial t} = -\left[\frac{\partial(\rho u u)}{\partial x} + \frac{\partial(\rho u v)}{\partial y}\right] - \frac{\partial p}{\partial x} + \frac{\partial \tau_{xx}}{\partial x} + \frac{\partial \tau_{xy}}{\partial y} \tag{2}$$

$$\frac{\partial(\rho v)}{\partial t} = -\left[\frac{\partial(\rho v u)}{\partial x} + \frac{\partial(\rho v v)}{\partial y}\right] - \frac{\partial p}{\partial y} + \frac{\partial \tau_{yx}}{\partial x} + \frac{\partial \tau_{yy}}{\partial y} \tag{3}$$

Energy equation:
$$\frac{\partial(\rho h)}{\partial t} + \frac{\partial(\rho u h)}{\partial x} + \frac{\partial(\rho v h)}{\partial y} = \frac{\partial\left(\lambda_f \partial T_f\right)}{\partial x^2} + \frac{\partial\left(\lambda_f \partial T_f\right)}{\partial y^2} + \sum_i\left[\frac{\partial}{\partial x}\left(h_i \rho D_{m,i}\frac{\partial Y_i}{\partial x}\right) + \frac{\partial}{\partial y}\left(h_i \rho D_{m,i}\frac{\partial Y_i}{\partial y}\right)\right] + \sum_i h_i R_i \tag{4}$$

Species equation:
$$\frac{\partial(\rho Y_i)}{\partial t} + \frac{\partial(\rho Y_i u)}{\partial x} + \frac{\partial(\rho Y_i v)}{\partial y} = \frac{\partial}{\partial x}\left(\rho D_{m,i}\frac{\partial Y_i}{\partial x}\right) + \frac{\partial}{\partial y}\left(\rho D_{m,i}\frac{\partial Y_i}{\partial y}\right) + R_i \tag{5}$$

Energy equation for the solid walls:
$$\frac{\partial(\lambda_s \partial T_s)}{\partial x^2} + \frac{\partial(\lambda_s \partial T_s)}{\partial y^2} = \frac{\partial(\rho_s c_s T_s)}{\partial t} \tag{6}$$

where u and v are the x and y components of the flow velocity, respectively; P is the fluid pressure; τ is the stress on the fluid; $D_{m,i}$ is the mass diffusion coefficient of species i; ρ and ρ_s are the densities of the fluid and solid wall, respectively; Y_i, h_i, and R_i are the

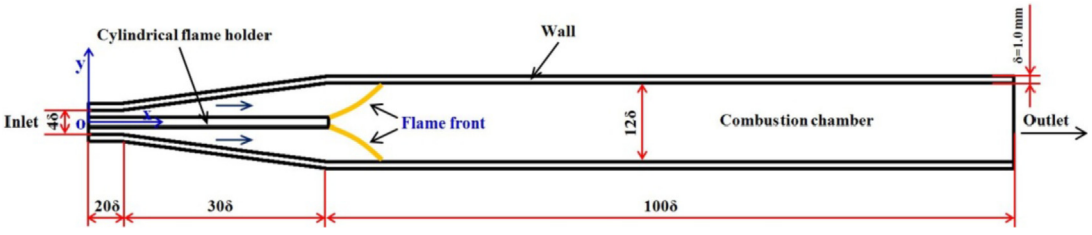

Fig. 1. Cross-section schematic of the meso-scale diverging combustor with cylindrical flame holder.

mass fraction, formation enthalpy, and generation/consumption rate of species *i*, respectively; λ_f and λ_s are the thermal conductivities of the fluid and solid wall, respectively; T_f and T_s are the fluid and solid wall temperatures, respectively.

2.3. Computational scheme

Methane and air are used as fuel and oxidizer, respectively. Two cases are adopted to study the heat exchange of flame holder on flame dynamics. One is the flame holder with heat exchange (FHW); the another is the flame holder without heat exchange (FHO, *i.e.*, the wall temperature of the flame holder is set as 300 K). The CFD software Fluent 14.0 is applied to solve the momentum, mass, energy, and species conservation equations [24]. The detailed C1 chemistry mechanism of CH_4/air combustion reaction (18 species and 58 reversible reactions) is adopted [25], and the thermodynamic and transport properties of the reaction species are obtained from the CHEMKIN databases [26]. The present work adopts the multi-component model. As the Soret (second-order) diffusion is generally much smaller than the Fickian (first-order) diffusion for methane/air premixed flame [27], the Soret effect is ignored here. The following are the boundary conditions in the current simulation:

In addition, grid independency is checked. It is found that the cell size of 75 μm is sufficiently fine to capture the flame structure [23]. Further refinement is conducted on the meshes around the cylindrical flame holder. Considering both computation accuracy and cost, a time step of 1.0×10^{-6} s is adopted. Our previous publications [19,20] have indicated that the time step of 1.0×10^{-6} s is small enough to capture the flame behaviors in the meso-scale combustors. The flammability limits via experiments and simulation were compared to validate the accuracy of the present numerical model [23]. In addition, the similar numerical models and methods were also adopted to simulate the meso-scale combustors with bluff body or cavity, and a good agreement between simulation results and experimental observations were achieved [18–20,30]. The present computational work was carried out as the flow path indicated in Fig. 2.

3. Results and analysis

Our previous work has confirmed that the normalized isolines of 10% maximum mass fraction of HCO (Y_{HCO}) can be used to mark the flame front appropriately [23]. Here the flame front near the holder is defined as flame root, and that near the combustor wall is defined as flame top.

3.1. Flame characteristics in FHW

3.1.1. Flame behaviors in FHW

Fig. 3 indicates that the flame root is anchored at a more upstream location, and the flame front presents a funnel-shape *(i.e.*, "V" shape). The height of the flame (the vertical distance between the flame root and top) is short (~2.0 mm). The heat release rate (HRR) is larger near the flame top. This is mainly ascribed to a larger flame stretch at this location. Additionally, it is found that the flow velocity near the flame holder is larger and there is a recirculation zone near the upstream combustor wall.

3.1.2. Heat exchange effect of flame holder

Fig. 4 quantitatively shows the heat flux distribution characteristic of flame holder. A positive value means the heat flux enters the flame holder and a negative value means heat flux leaving the holder. The fresh mixture is preheated by the vertical wall of flame holder before ignition (the zone of negative value in Fig. 4a). Once ignited (just at the position of flame front), the flame holder is heated by the burnt gas of high temperature behind the flame front (the zone of positive value in Fig. 4a). Fig. 4b shows that nearly the whole upper wall of flame holder is cooled by the gaseous mixture. On the whole, the heat flux for preheating fresh mixture is 1.25 W, which occupies 84.5% of the whole heat flux that enters the flame holder, as shown in Fig. 4c.

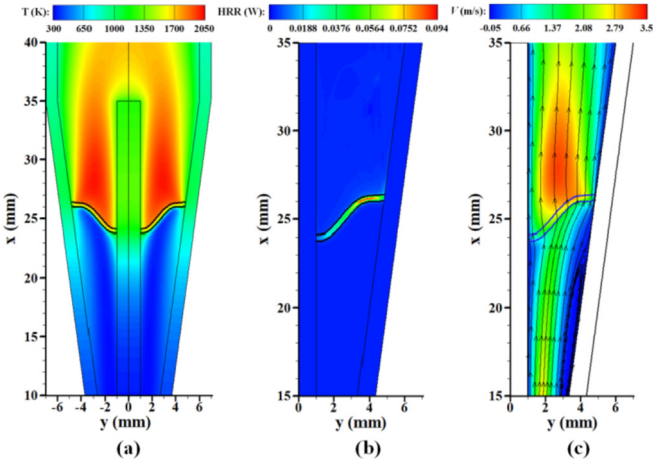

Fig. 3. The temperature filed (a), heat release rate (b), and flow field and streamlines (c) overlaid with 10% maximum Y_{HCO} isoline (black solid lines) in FHW (the flame holder with heat exchange).

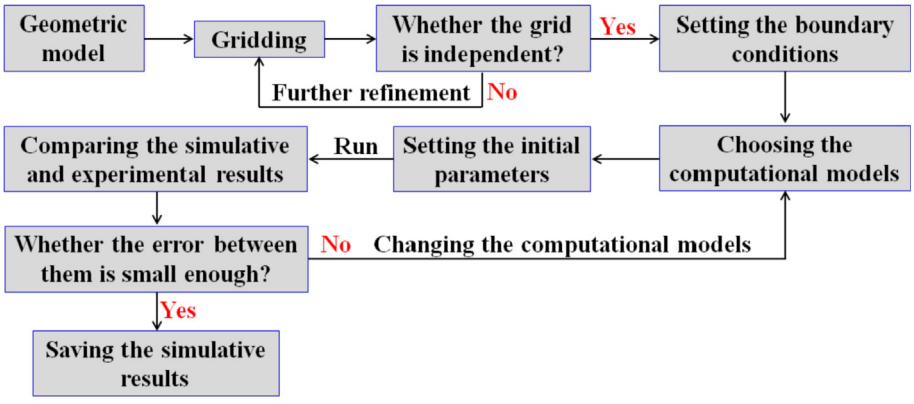

Fig. 2. The flow chart of the methodology used in the present simulation.

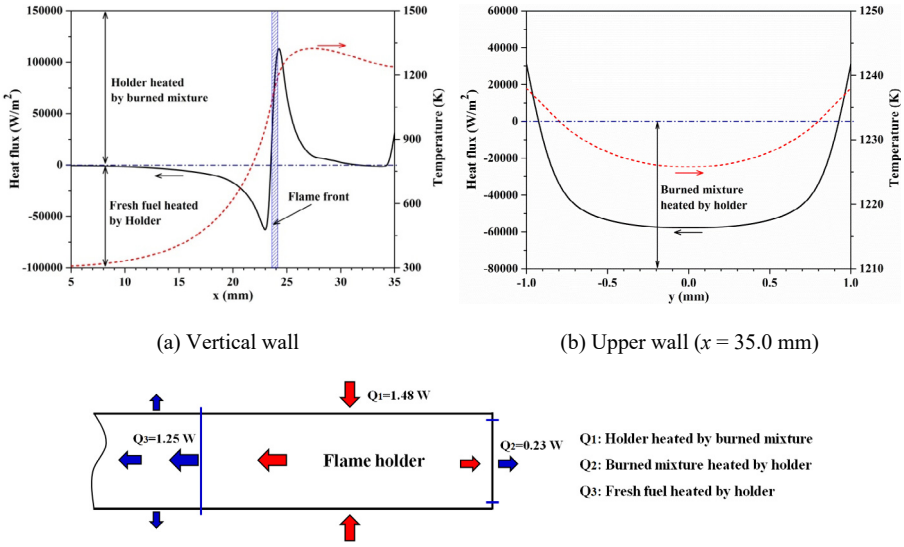

Fig. 4. Profiles of temperature and heat flux that enters the flame holder for the vertical wall (a) and upper wall (b) of flame holder, and the schematic of the heat transfer networks of flame holder (c).

3.1.3. *The effect of conjugate heat exchange on flame front*

Fig. 5 demonstrates the HRR and temperature profiles along the centerline of flame front. It can be seen that there exists a zone where the temperature remains constant (T_f) near the middle of the flame front. Therefore, three zones can be identified via normalizing the flame temperature by T_f: (1) the quenching zone (Z_q): the zone near the flame holder or combustor wall which features a drastic decreasing temperature. The conjugate heat exchange between the flame and solid wall leads to heat loss of the flame, so the flame temperature is lower than T_f; (2) the free reaction zone (Z_f): the zone near the middle of the flame front. The incoming fresh mixture is neither preheated by the flame holder or upstream combustor wall of high temperature nor cooled down by the heat loss, so an almost un-stretched laminar flame is generated, and hence the temperature keeps the same; (3) the enhanced reaction zone (Z_e) with a temperature higher than T_f, which means that the combustion within this zone may be more intense. This zone adjoining with the Z_f may be induced by the larger positive flame stretch due to the irregular flow field. Since the flame in Z_e is the conventional free propagation structure, a positive flame stretch is beneficial for the burning rate and intensity.

Fig. 5 also shows the HRR in Z_e is the largest among them while the HRR in Z_q is smaller due to the heat loss. In Z_f the HRR increases along the centerline of the flame front towards combustor wall. This may be caused by the structure characteristics of the flow field along the flame front, which can affect the distributive characteristics of reaction species via both convection and diffusion modes. This is different from the flame in the combustor with open space [31]. The downstream part of flame in Ref. [31] is nearly parallel to the streamline. This means that the reaction species enter the reaction zone mainly by the diffusion mode [16].

In order to further quantitatively analyze the heat exchange effect of flame holder on the flame, Fig. 6 shows the mass fractions of four key radicals along the paths of L_1 (very near the flame holder) and L_2 (near the middle of flame front), which are shown in

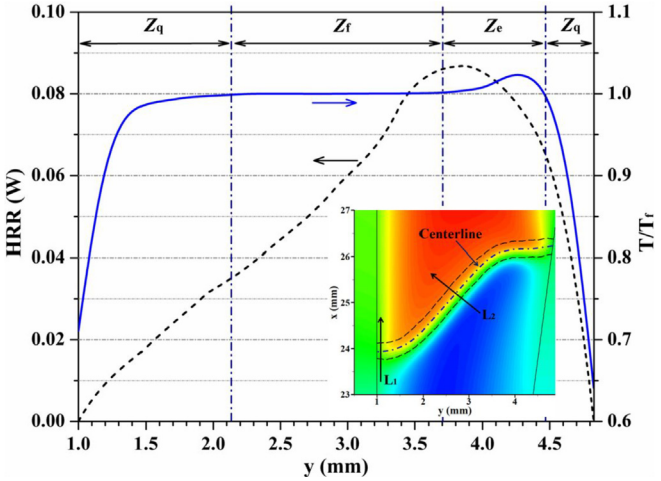

Fig. 5. Heat release rate and normalized gas temperature along the centerline of the flame front (bold dash-dot line in the insert).

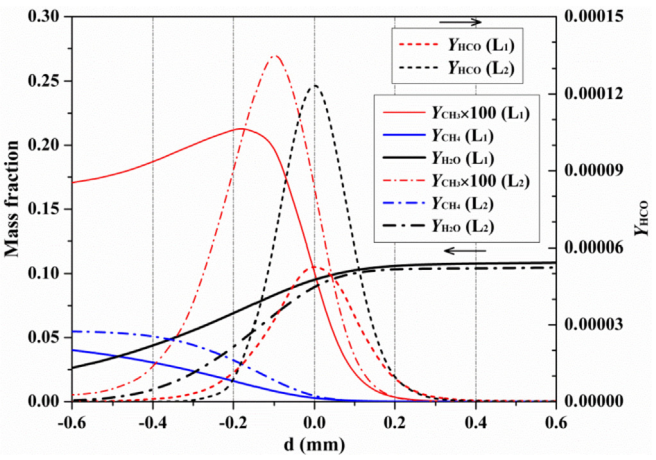

Fig. 6. Mass fraction distributions of HCO, CH_3, CH_4, and H_2O along the paths of L_1 in Z_q (very near the flame holder) and L_2 in Z_f (near the middle of flame front, see Fig. 4) (d = 0.0 mm is the center of flame front).

Fig. 5 (the positive direction towards the reaction products). It can be seen the mass fraction of CH_3 (an important intermediate species of initiation reaction) at L_1 is obvious larger than that at L_2 just before the flame front, which means that the initiation reactions (such as $CH_4 + O_2 = CH_3 + HO_2$) are more intense at L_1, so the methane is consumed and H_2O is produced earlier in a more upstream location. This is because the incoming fresh mixture at L_1 can be well preheated by the flame holder nearby. Fig. 6 also indicates that the thickness of the flame front (see Y_{HCO} profiles in Fig. 6) in Z_q is larger than that in Z_f due to the heat loss to the flame holder.

3.2. Flame dynamics in FHO

3.2.1. Pulsating flame in FHO

When the heat exchange of flame holder is absent, the flame root obviously shifts downstream and even stays at a more downstream location in comparison with the flame top. As a result, the flame front presents a cone shape (i.e., "Λ" shape) (Fig. 7), which is opposite with that in FHW (see Fig. 3). This indicates that the heat exchange of flame holder has a significantly anchoring effect on flame root. Unexpectedly, the flame in FHO pulsates up and down instead of remaining stationary. Fig. 7I shows the first half of pulsating mode (the flame root propagates upstream) in FHO. It can be seen that the flame root and top both shift upstream, but their moving speeds are different. Thereafter, the flame root shifts downstream with a slower moving speed than that in the first half (see Fig. 7II).

3.2.2. Mechanisms of flame pulsation

As known, the movement of the flame is determined by the relative magnitude between the flame speed and the corresponding flow velocity. When the flame speed is larger, the flame propagates upstream; when the flame speed is smaller, the flame propagates downstream. The heat transfer effect of the flame holder can affect both the local flow velocity and flame speed. On the one hand, the heat transfer effect can influence the flow structure (including the flow magnitude and direction) via thermal

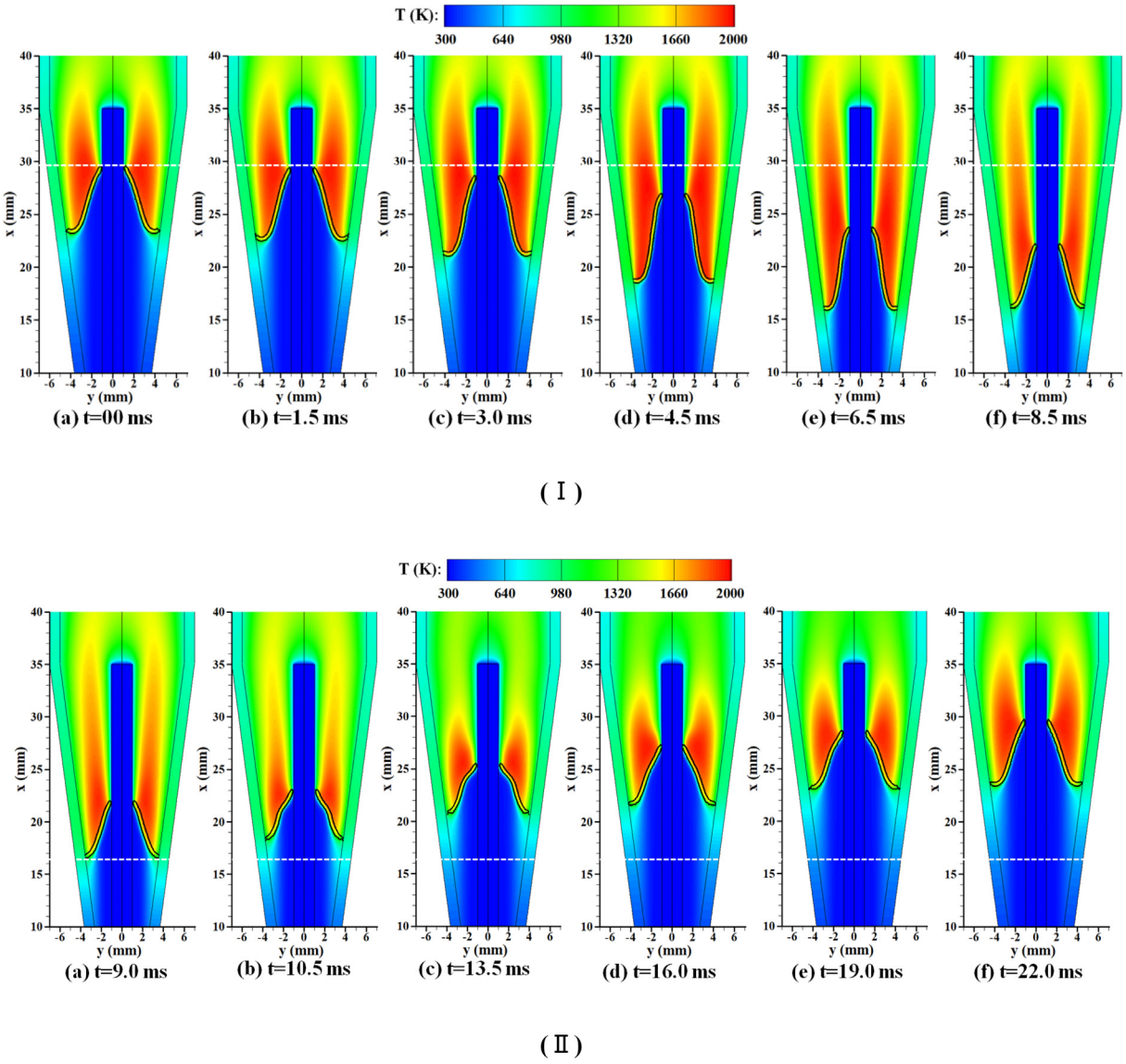

Fig. 7. The temperature field overlaid with 10% maximum Y_{HCO} isoline (black solid lines) at the first half of pulsating mode (I, the flame root propagates upstream) and second half of pulsating mode (II, the flame root propagates downstream) in FHO (the flame holder without heat exchange).

expansion effect. On the other hand, the heat transfer effect can affect the flame speed via influencing the preheated temperature of fresh fuel mixture and the stretch rate. The pulsating mechanisms of the flame will be systematically discussed via quantitatively or semi-quantitatively comparing the relative magnitude between the flame speed and the local flow velocity.

Fig. 8 shows that there exists a recirculation zone near the combustor wall, and it decreases with time. The recirculation zone results in a more irregular flow field near the flame top, which significantly influences the flame stretch around it. The flow velocity near the flame top is obviously smaller than that near the flame root. In addition, the flow velocity near the flame front increases during this stage mainly due to the decrease of flow area. At the meantime, a narrower flow space also means a larger heat loss through the closer combustor wall. These characteristics significantly affect the local flame speed, the local flow velocity, and the heat exchange of combustor wall.

It is known that the stretched flame speed (S) under a small stretch is defined as follows [27]:

$$S = S_u - Lk \tag{7}$$

where S_u is the unstretched flame speed; L is the Markstein length, which is nearly constant for methane/air mixture under a certain equivalence ratio (a positive value here, ~0.1×10^{-3} [32]); k is the flame stretch rate ($k = k_s + k_c$), as the contribution of the latter (k_c) to flame stretch is practically negligible because of a smooth and flat flame behavior [32,33], $k \approx k_s$. The strain rate (k_s) is [32]:

$$k_s = -n_x n_y \left[\frac{\partial u}{\partial y} + \frac{\partial v}{\partial x}\right] - n_x^2 \frac{\partial u}{\partial x} - n_y^2 \frac{\partial v}{\partial y} \tag{8}$$

where u is the x-component of flow velocity; v is the y-component of flow velocity; n is the normal direction of flame front towards the reactions; $\partial u/\partial x$ and $\partial u/\partial y$ are the velocity gradients of u at x and y directions, respectively; $\partial v/\partial x$ and $\partial v/\partial y$ are the velocity gradients of v at x and y directions, respectively. It is well known that the stable flame must satisfy the condition of $|S| = |V_n|$ (the flame speed (S) is equal to the local flow velocity normal to the flame front (V_n)).

Fig. 9 shows that $V_n = V_{local} \times \cos\theta$ (V_{local} is the local flow velocity, θ is the acute angle between V_{local} and V_n). $\theta = |\theta_{flow} + \theta_{flame} - 180°|$ (θ_{flow} is the angle between flow direction and positive direction of y-axis; θ_{flame} is the angle between normal direction of flame front towards unburned reactants and positive direction of y-axis).

Along the upstream boundary of flame root towards middle of flame front, θ_{flow} decreases while θ_{flame} increases (Fig. 10a), which results in a decreasing θ (Fig. 10b). According to the equations above, Fig. 10b shows that V_n slightly increases along the upstream boundary of the flame root. In addition, Fig. 10c presents that k_s slightly increases, which induces a slight increase in the flame speed. At $t = 0.0$ ms, the flame speed (S) is larger than V_n (Fig. 10b), which makes the flame start to shift upstream. Whereafter, V_n is the smallest at $t = 5.5$ ms, so the flame speed (S) is still larger. Moreover, the larger difference between S and V_n probably leads to the faster moving speed of the flame root near $t = 5.5$ ms (please refer to Fig. 7I). Over time, the difference between S and V_n becomes smaller and smaller, and V_n will be equal to S at a certain location. However, the inertia of the flame makes it shift upstream further. At

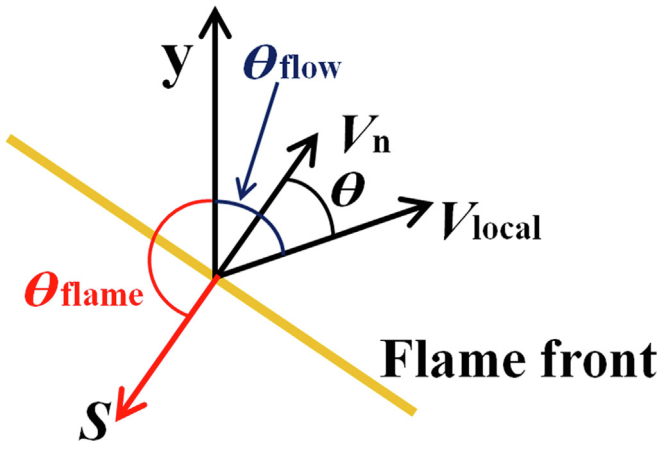

Fig. 9. The schematic of the flow velocity and flame speed at one point of the flame front.

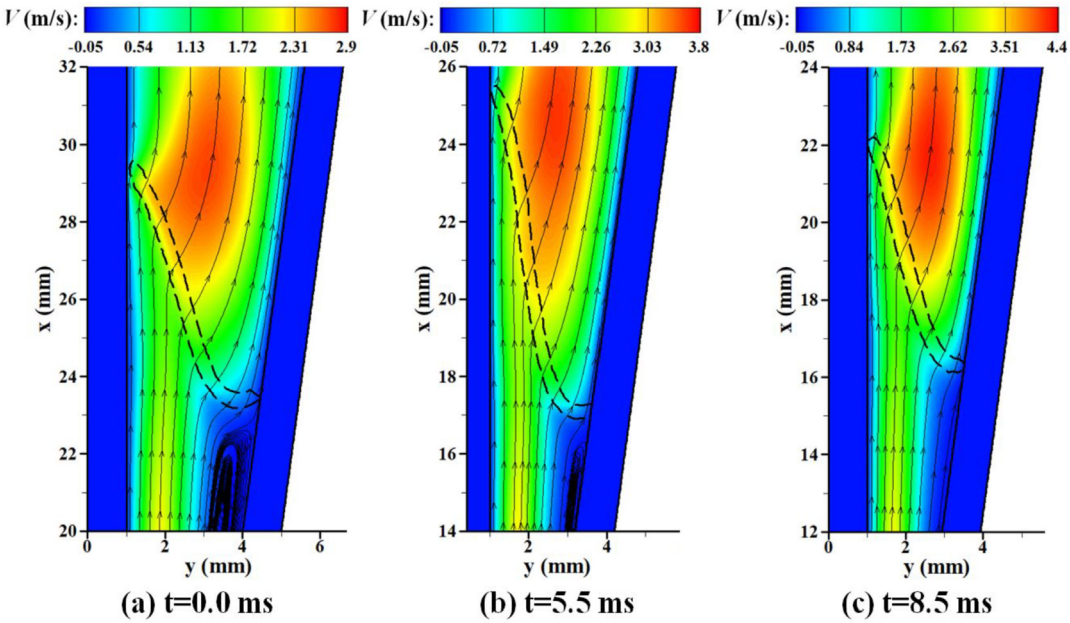

Fig. 8. The flow filed and streamlines overlaid with 10% maximum Y_{HCO} isoline (black dashed lines) at the first half of pulsating mode (the flame root propagates upstream) in FHO.

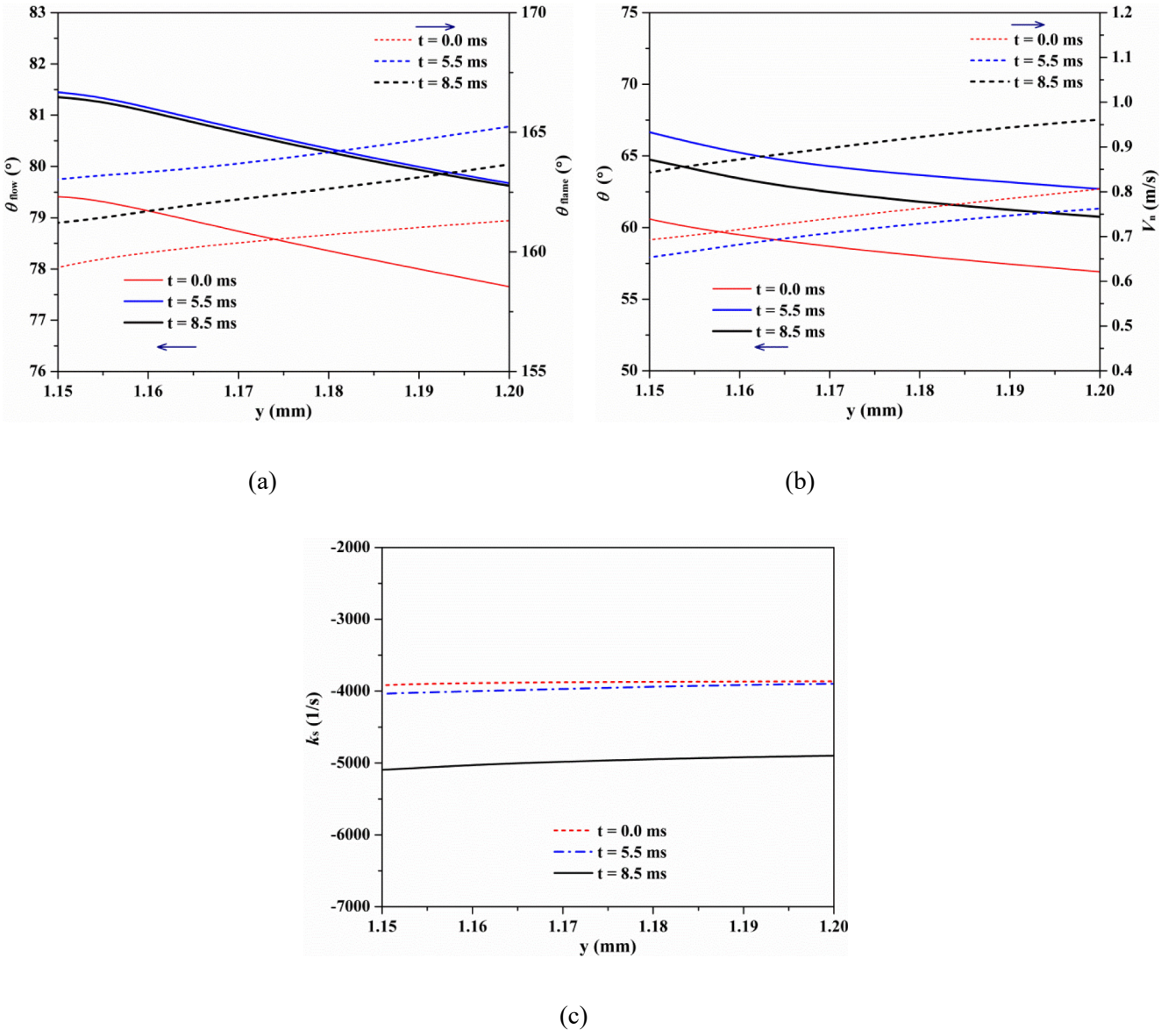

Fig. 10. θ_{flow} and θ_{flame} (a),θ and V_n (b), and flame strain (c) along the upstream boundary of flame root (*i.e.*, upstream boundary of 10% maximum Y_{HCO} isoline) for different time points.

$t = 8.5$ ms, even though $|k_s|$ is large, a larger V_n impedes the upstream movement of the flame root. After that, the flame starts to shift downstream.

For the flame top, along the upstream boundary of the flame top towards the middle of the flame, θ_{flow} decreases while θ_{flame} increases (Fig. 11a). As a result, θ nearly maintains the same at $t = 0.0$ ms and $t = 5.5$ ms whereas it decreases at $t = 7.5$ ms (Fig. 11b). However, V_n still increases along the upstream boundary because it is mainly determined by the magnitude of the flow velocity. In addition, V_n at the flame top is obviously smaller than that at the flame root. Fig. 11c shows that the decreasing k_s results in an increase of the flame speed.

Furthermore, as the flame top is near the combustor wall, it is inevitably influenced by the heat exchange of the combustor wall. In order to get insights into this effect, the distributive characteristics of the temperature and the heat flux along the inner surface of combustor wall are obtained, as shown in Fig. 12a. It can be seen that the inner wall temperature and the heat flux that enters the combustor wall at $t = 5.5$ ms are obviously the largest among them even though the heat loss to environment is also the largest (Fig. 12b). This is probably because the flame front at $t = 5.5$ ms is the longest and its upstream part is the closest to the combustor wall. As a result, the gaseous mixture is preheated better (see Fig. 12c, the preheated zone of flame front is near the upstream boundary), which is beneficial for the increase in the flame speed.

Therefore, at $t = 0.0$ ms, even though S is small (see Figs. 11c and 12c), V_n is even smaller (Fig. 11b), so the flame top starts to move upstream. When the time arrives 5.5 ms, V_n is bigger (Fig. 11b) while S also increases to a bigger value, so the flame speed (S) may be still larger than V_n. Similar to the flame root, V_n will be equal to S at a certain point, but the inertia makes the flame shift upstream further. At $t = 7.5$ ms, the larger V_n compared with S makes the flame top start to shift downstream.

In a similar way, $|S| \leq |V_n|$ leads to the downstream movement of the flame front in the second half of pulsating mode (the flame propagates downstream).

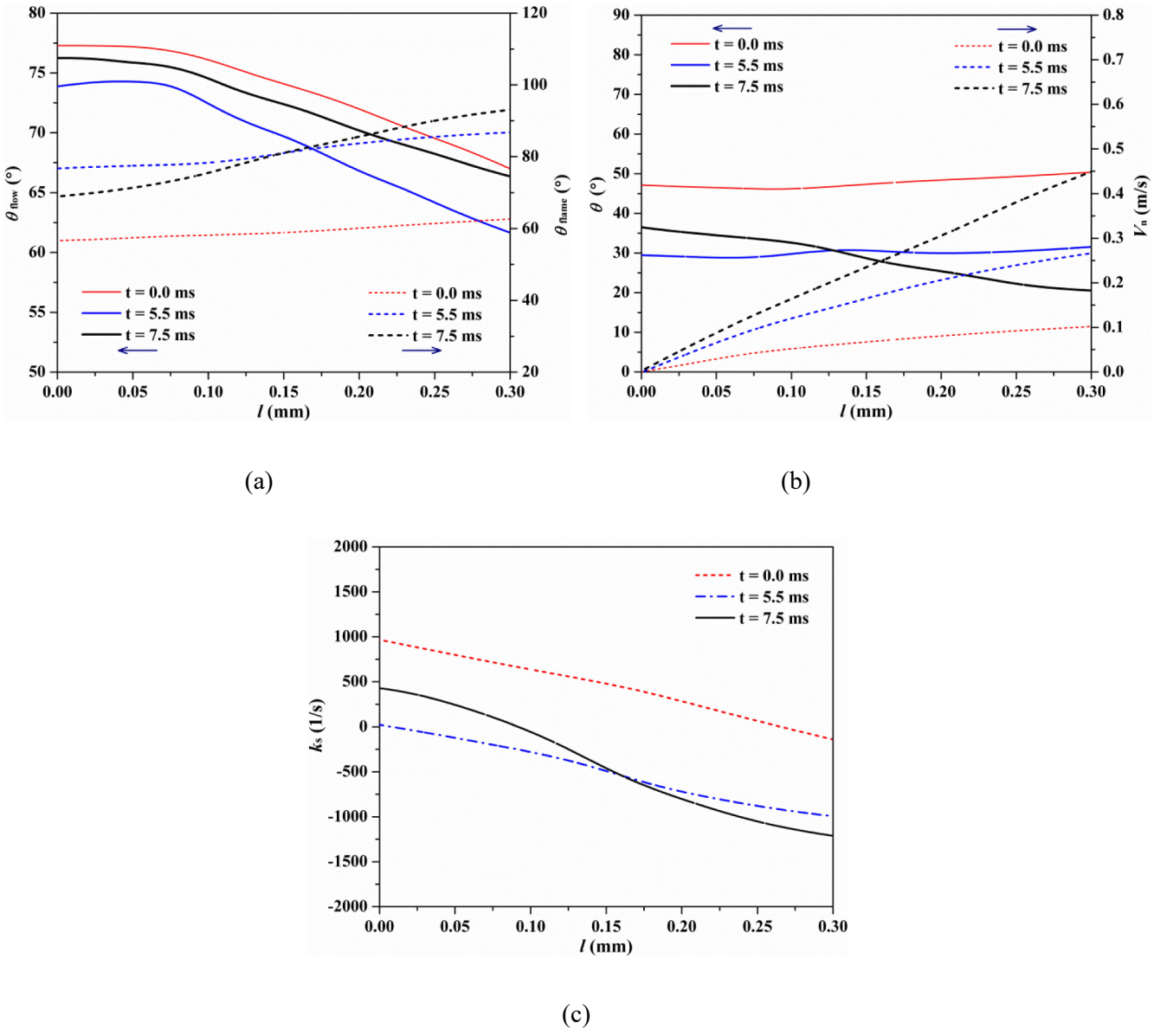

Fig. 11. θ_{flow} and θ_{flame} (a), θ and V_n (b), and k_s (c) along the upstream boundary of flame top (*i.e.*, upstream boundary of 10% maximum Y_{HCO} isoline) for different time points (l is the curve distance to the combustor wall).

4. Discussion

Even though the effect of the conjugate heat exchange of the solid wall on the flame stabilization in the combustors with a constant channel width has been widely investigated [10–22], the studies on improving the flame stabilization in the variable channel width were rare in literatures. The present study quantitatively investigates the effect of heat exchange of flame holder on the flame stabilization in the tube combustor with variable channel width. It is found that the flame by the flame holder with the heat exchange can remain stable, and a majority of the heat flux that enters the flame holder is used to preheat the fresh mixture. However, when the heat exchange effect of flame holder is absent, the flame height obviously increases, and the flame pulsates with a high frequency. In Ref. [31], the flame can still remain stable when the heat exchange of cylindrical bluff-body is absent in a combustion chamber with constant channel width, which is different with the present results. This indicates that the anchoring effect of the heat exchange of flame holder on the flame in the variable channel width may be more important than that in the constant channel width. Therefore, it is very necessary to investigate the flame dynamics in the combustion chamber with variable channel width. It should be pointed out that the present work only studied the flame propagation behavior at a typical case, maybe the characteristic parameters of the flame (such as the flame height, pulsating frequency, and so on) at different operating conditions are different, but we believe that the present conclusion can still be suitable for other cases. In summary, the heat exchange of flame holder can significantly improve the flame stability in the diverging combustor.

5. Conclusions

The current work numerically studies the effect of the heat exchange of flame holder on the premixed flame in a diverging channel. It is found that the conjugate heat exchange between the

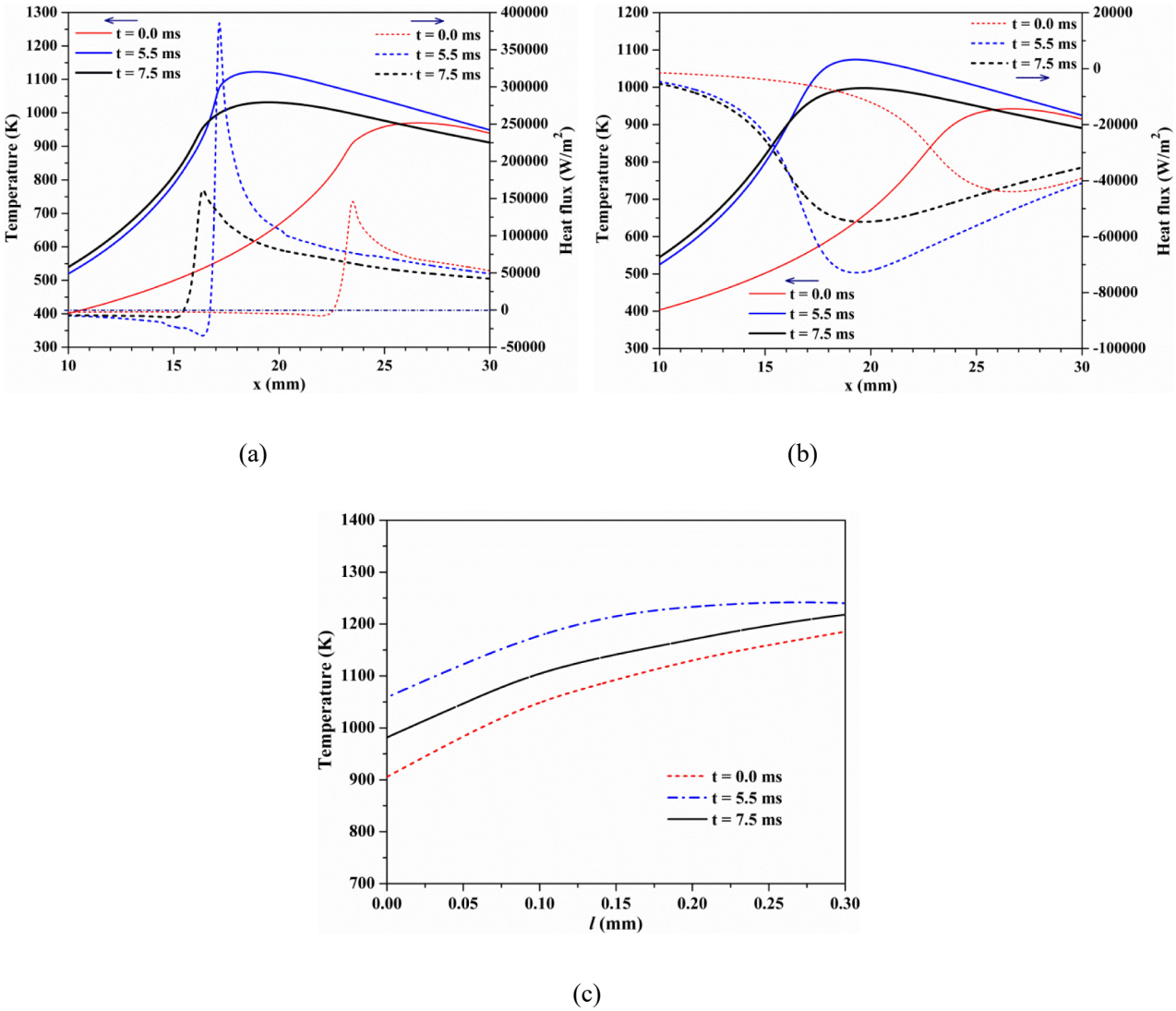

Fig. 12. Profiles of temperature and heat flux that enters the wall along the inner surface (a) and outer surface (b) of combustor wall in diverging section, and gas temperature (c) along the upstream boundary of the flame top for different time points.

flame and solid wall has a significant effect on the flame topology structure and flame stability. The flame anchored by the flame holder with the heat exchange can remain stable and present a "V" shape. The height of the flame is ~2.0 mm. In addition, a majority (~84.5%) of the heat flux that enters the flame holder is used to preheat the incoming fresh mixture, which can induce and enhance the initiative reactions. Interestingly, a reaction zone with constant temperature (T_f) is found, which is defined as a free reaction zone (Z_f), and the quenching zone (Z_q) and the enhanced reaction zone (Z_e) are also defined based on T_f. However, when the heat exchange of flame holder is absent, the flame pulsates up and down instead of remaining stable (the pulsating frequency is ~45.5 HZ), and the flame shows a cone "Λ" shape. Then, the pulsating mechanisms of the flame are quantitatively analyzed in terms of local flow velocity, the angle between flow direction and flame front, and stretch rate. In one word, a larger flame speed compared with V_n results in the upstream movement of the flame. On the contrary, a larger V_n pushes the flame downstream. This is a dynamic process where the flame speed self-adjusts to match V_n. The heat exchange of flame holder can significantly suppress the flame instability and improve the flame anchoring performance.

Declaration of competing interest

The authors declare that they have no known competing financial interests or personal relationships that could have appeared to influence the work reported in this paper.

CRediT authorship contribution statement

Jianlong Wan: Conceptualization, Methodology, Formal analysis, Investigation, Data curation, Writing - original draft, Visualization. **Haibo Zhao:** Writing - review & editing, Validation, Supervision.

Acknowledgements

This work was supported by the National Natural Science Foundation of China (Nos. 51706080) and the Fundamental Research Funds for the Central Universities (2019kfyXJJS110).

References

[1] Ju Y, Maruta K. Microscale combustion: technology development and fundamental research. Prog Energy Combust Sci 2011;37:669–715.
[2] Maruta K, Kataoka T, Kim NI, Minaev S, Fursenko R. Characteristics of combustion in a narrow channel with a temperature gradient. Proc Combust Inst 2005;30:2429–36.
[3] Alipoor A, Mazaheri K. Combustion characteristics and flame bifurcation in repetitive extinction-ignition dynamics for premixed hydrogen-air combustion in a heated micro channel. At Energ 2016;109:650–63.
[4] Xu B, Ju Y. Experimental study of spinning combustion in a meso-scale divergent channel. Proc Combust Inst 2007;31:3285–92.
[5] Wan JL, Shang C, Zhao H. Dynamics of methane/air premixed flame in a meso-scale diverging combustor with/without a cylindrical flame holder. Fuel 2018;232:659–65.
[6] Deshpande AA, Kumar S. On the formation of spinning flames and combustion completeness for premixed fuel–air mixtures in stepped tube micro-combustors. Appl Therm Eng 2013;51:91–101.
[7] Akram M, Kumar S. Experimental studies on dynamics of methane–air premixed flame in meso-scale diverging channels. Combust Flame 2011;158:915–24.
[8] Kuo CH, Ronney PD. Numerical modeling of non-adiabatic heat-recirculating combustors. Proc Combust Inst 2007;31:3277–84.
[9] Federici JA, Vlachos DG. A computational fluid dynamics study of propane/air microflame stability in a heat recirculation reactor. Combust Flame 2008;153:258–69.
[10] Veeraragavan A. On flame propagation in narrow channels with enhanced wall thermal conduction. At Energ 2015;93:631–40.
[11] Hashemi SM, Hashemi SA. Flame stability analysis of the premixed methane-air combustion in a two-layer porous media burner by numerical simulation. Fuel 2017;202:56–65.
[12] Li J, Wang Y, Shi J, Liu X. Dynamic behaviors of premixed hydrogen–air flames in a planar micro-combustor filled with porous medium. Fuel 2015;145:70–8.
[13] Ning D, Liu Y, Xiang Y, Fan A. Experimental investigation on non-premixed methane/air combustion in Y-shaped meso-scale combustors with/without fibrous porous media. Energy Convers Manag 2017;138:22–9.
[14] Peng Q, J E, Chen J, Zuo W, Zhao X, Zhang Z. Investigation on the effects of wall thickness and porous media on the thermal performance of a non-premixed hydrogen fueled cylindrical micro combustor. Energy Convers Manag 2018;155:276–86.
[15] Bani S, Pan J, Tang A, Lu Q, Zhang Y. Numerical investigation of key parameters of the porous media combustion based Micro-Thermophotovoltaic system. At Energ 2018;157:969–78.
[16] Kedia KS, Ghoniem AF. The anchoring mechanism of a bluff-body stabilized laminar premixed flame. Combust Flame 2014;161:2327–39.
[17] Yang WM, Chou SK, Shu C, Xue H, Li ZW, Li DT, et al. Microscale combustion research for application to micro thermophotovoltaic systems. Energy Convers Manag 2003;44:2625–34.
[18] Wan JL, Fan AW, Maruta K, Yao H, Liu W. Experimental and numerical investigation on combustion characteristics of premixed hydrogen/air flame in a micro-combustor with a bluff body. Int J Hydrogen Energy 2012;37:19190–7.
[19] Wan JL, Fan AW, Liu Y, Yao H, Liu W, Gou XL, et al. Experimental investigation and numerical analysis on flame stabilization of CH_4/air mixture in a meso-scale channel with wall cavities. Combust Flame 2015;162:1035–45.
[20] Wan JL, Fan AW, Yao H, Liu W. Experimental investigation and numerical analysis on the blow-off limits of premixed CH_4/air flames in a meso-scale bluff-body combustor. At Energ 2016;113:193–203.
[21] Baigmohammadi M, Sarrafan Sadeghi S, Tabejamaat S, Zarvandi J. Numerical study of the effects of wire insertion on CH_4 (methane)/AIR pre-mixed flame in a micro combustor. At Energ 2013;54:271–84.
[22] Yang WM, Jiang DY, Chua KYK, Zhao D, Pan JF. Combustion process and entropy generation in a novel microcombustor with a block insert. Chem Eng J 2015;274:231–7.
[23] Wan JL, Shang C, Zhao H. Anchoring mechanisms of methane/air premixed flame in a meso-scale diverging combustor with cylindrical flame holder. Fuel 2018;232:591–9.
[24] Fluent 14.0. User's guide. 2011. Canonsburg, PA, https://support.ansys.com/portal/site/Ansys-CustomerPortal.
[25] Bilger RW, Starner SH. On reduced mechanisms for methane air combustion in nonpremixed flames. Combust Flame 1990;80:135–49.
[26] Kee RJ, Grcar JF, Smooke MD, Miller JA. Sandia national laboratories report, SAND85-8240. 1994. https://www.sandia.gov/.
[27] Law CK. Combustion physics. Cambridge: Cambridge University press; 2006.
[28] Holman JP. Heat transfer. ninth ed. New York: McGraw-Hill; 2002.
[29] Ma Q, Fang R, Xiang L. Handbook of thermo-physical properties. Bejing: China Agricultural Machinery Press; 1986 (in chinese).
[30] Wan JL, Fan AW. Effect of channel gap distance on the flame blow-off limit in meso-scale channels with cavities for premixed CH_4/air flames. Chem Eng Sci 2015;132:99–107.
[31] Miguel-Brebion M, Mejia D, Xavier P, Duchaine F, Bedat B, Selle L, et al. Joint experimental and numerical study of the influence of flame holder temperature on the stabilization of a laminar methane flame on a cylinder. Combust Flame 2016;172:153–61.
[32] Kedia KS, Ghoniem AF. The blow-off mechanism of a bluff-body stabilized laminar premixed flame. Combust Flame 2015;162:1304–15.
[33] Wan JL, Cheng X. Numerical investigation of the local extinction and re-ignition mechanisms of premixed flame in a micro combustor with a flame holder and preheating channels. Fuel 2020;264:116837.

Nomenclature

$D_{m,i}$: Mass diffusion coefficient of species i, m^2/s
FHO: Flame holder without heat exchange
FHW: Flame holder with heat exchange
h: Enthalpy of the fluid, kj/kg
h_i: Formation enthalpy of species i, kj/kg
h_s: Natural convection coefficient, $W \cdot m^{-2} \cdot K^{-1}$
HRR: Heat release rate, W
k: Stretch rate, 1/s
k_c: Curvature rate, 1/s
k_s: Strain rate, 1/s
L: Markstein length, m
n: Normal direction of flame front towards the reactions
P: Pressure of the fluid, Pa
q: Heat loss rate, W/m^2
R_i: Generation/consumption rate of species i, kg/s
Re: Reynolds number
S: Stretched flame speed, m/s
S_u: Unstretched flame speed, m/s
t: Time, s
T_f: Constant temperature value near the middle of the flame front, K
T_g: Fluid temperature, K
T_s: Solid material temperature, K
$T_{w,o}$: Surface temperature of outer wall, K
T_∞: Ambient temperature, K
u: x-component of the flow velocity, m/s
v: y-component of the flow velocity, m/s
V_{local}: Local flow velocity, m/s
V_n: Local flow velocity normal to the flame front, m/s
x: Vertical distance from the origin of the coordinates, m
y: Horizontal distance from the origin of the coordinates, m
Y_i: Mass fraction of species i
Z_e: Enhanced reaction zone
Z_f: Free reaction zone
Z_q: Quenching zone

Greeks

ε_s: Surface emissivity
λ_f: Thermal conductivities of the fluid, $W \cdot m^{-1} \cdot K^{-1}$
λ_s: Thermal conductivities of the solid wall, $W \cdot m^{-1} \cdot K^{-1}$
σ_s: Stephan-Boltzmann constant, $W \cdot m^{-2} \cdot K^{-4}$
ρ: Density of the fluid, kg/m^3
ρ_s: Density of the solid wall, kg/m^3
θ: Acute angle between V_{local} and V_n, °
θ_{flame}: Angle between normal direction of flame front towards unburned reactants and positive direction of y-axis, °
θ_{flow}: Angle between flow direction and positive direction of y-axis